ISSN NO. 2320-5407

Journal homepage: http://www.journalijar.com

INTERNATIONAL JOURNAL OF ADVANCED RESEARCH

RESEARCH ARTICLE

The synoptic patterns of widespread dust days in the northern Arabian Peninsula in summer

Adel Awad

Center of Excellence for Climate Change Research/Department of Meteorology, King Abdul Aziz University Jeddah, Saudi Arabia

Manuscript Info

Manuscript History:

Received: 22 December 2014
Final Accepted: 26 January 2015
Published Online: February 2015

Key words:

TOMS aerosol index; summer dust; synoptic patterns; northern Saudi Arabia

Corresponding Author

Adel Awad

Abstract

Using an aerosol index (AI) threshold for the TOMS satellite, dust episodes were detected and classified. The selected cases show that approximately 82% of the summer is dusty, while 9.3% of the summer experiences widespread dust episodes.

A statistical analysis of widespread dust episodes in summer demonstrated that there are four main synoptic patterns, which represent 52% of the cases over the northern Arabian Peninsula. In addition, a synoptic analysis of these main patterns shows that two factors control these cases: the scale of the pressure systems in the region and the interaction between the Azores high and Indian low pressure systems.

The frequency of a synoptic pattern is inversely proportional to the scale of the influence of the synoptic features over the Arabian Peninsula. Furthermore, a frequent pattern appeared when the Azores high pressure system was strong and dominant, while a less frequent pattern appeared when the Indian low pressure was strong and dominant and when a high-pressure belt was present over the northern region. Moreover, two moderate patterns whose frequency depended on the synoptic similarity to one of the extreme patterns occurred.

INTRODUCTION

The Arabian Peninsula experiences highly active dust and aerosol loading in summer (Smirnov et al., 2002; Kim et al., 2011; Maghrabi et al., 2011), when approximately 82% of the days are dusty (Awad 2014).

The atmospheric dust load requires suitable conditions for lifting and transferring dust from sources (Goudie and Middleton 2006). Although many studies have investigated the atmospheric conditions during dust events, most of these studies investigated the general conditions associated with particular cases, e.g., Mohalfi et al. 1998, Gkikas et al. (2012) and Awad and Mashat (2014-a), Awad et al. (2014).

Few studies have attempted to specify the synoptic patterns associated with dust episodes. For example, Hamidi et al. 2013 found that two types of systems accompany dust storms in the Middle East: the Shamal ("north wind" in Arabic) and frontal systems. The Shamal synoptic system is characterized by a high-pressure system over the Mediterranean region and a low-pressure system over southern Iran; a frontal system is a high-pressure system over southern Iran and a low-pressure system over the eastern Mediterranean region. Additionally, Barkan and Alpert 2008 described the synoptic pattern of Sahara dusty and non-dusty seasons using a threshold value from the TOMS aerosol index (TOMS AI) satellite. Moreover, Gkikas et al. 2012 used factor analysis and cluster analysis (Jolliffe 1986 and Manly 1986)to identify 322 aerosol episodes with unusually high aerosol days in the greater

Mediterranean basin; these episodes were classified into eight synoptic clusters. Furthermore, Awad and Mashat 2014-b used statistical analysis to identify the main synoptic patterns associated with widespread dust events that influenced the central and eastern Arabian Peninsula in spring.

Considering the temporal and spatial properties of dust events, the purpose of this work is to specify the main synoptic types of widespread summer dust cases in northern Saudi Arabia. The dust cases classified according to the value and distribution of a threshold of aerosol index (AI) data collected by the TOMS satellite over the northern Arabian Peninsula.

The paper is organized as follows. In section 2, the data are described. Section 3 presents the methodology. Section 4 examines the results and synoptic characteristics of the composition of the main widespread patterns. The final section contains a discussion and conclusions.

2. Data

The TOMS AI is one of the most important and long-term measurements of global atmospheric aerosols; absorbing aerosols over land and water can be detected (Herman et al., 1997; Torres et al., 1998). The TOMS AI is proportional to the optical depth and dust altitude (Mahowald et al. 2003), but a weak TOMS AI could represent a high amount of dust near the surface. To avoid this deficiency, a threshold value for the AI was used in this study (Hsu et al. 1999, Crosbie et al. 2014). Additionally, the threshold was used as a condition for selecting and classifying dust episodes (details are provided in the methodology section).

The data consist of 25 years of daily global measurements of UV radiances at three discrete wavelengths(340, 360, and 380 nm) collected from the TOMS instruments. The data cover November 1978 to September 2006, with a gap from May 1993 to July 1996.

The meteorological data are the sea-level pressure (SLP), the wind components at 850 hPa and 250 hPa, vertical motion at 500 hPa and geopotential heights at 850 hPa and 500 hPa during summer (June, July, and August) from 1979 to 2006. The meteorological data were collected from the NCEP/NCAR reanalysis dataset (Kalnay et al., 1996, Kistler et al., 2001),which has a horizontal spatial resolution of 2.5° × 2.5°. The study domain is delimited by 0°E-70°E and 10°N-50°N.

3. Methodology

The dust episodes were selected using a specific value (threshold) of the TOMS AI data and were classified depending on the number of grid points that reached this value within the “checking zone” area. The checking zone is the area that represents the northern Arabian Peninsula and is delineated by 26°N to 32°N and 35°E to 48°E (rectangle in figure 1-a). The threshold value represents the average aerosol index plus half of the standard deviation for all episodes that have an AI value greater than zero and at least one grid point within the checking zone. After the threshold value was specified, i.e. AI of 2.0, it was used to select all the summer dust episodes, i.e., the cases that have at least one grid point that reaches the threshold . See Awad and Mashat (2014-a) and Awad et al. (2014) for details. In addition, the selected case was classified as a widespread case "WS" if at least 70% of the total grid points (73 grid points) reached the threshold value of the checking zone.

After the widespread dust episodes were selected, the SLP data of these cases were statistically analyzed using the empirical orthogonal function (EOF); the synoptic features that represented the first four EOF modes were analyzed in this paper. For details, please refer to Awad and Mashat (2014-b).

4. Results

Applying the methodology within the checking zone for all summer days yielded 1955 dust cases, which represent 82.0% of the studied summer period. Of the cases, 182 were classified as widespread “WS”.

The previous ratios indicate that summer is a potential dust season and that most of the dust episodes were not widespread (widespread episodes only represent 9.3% of the total dust episodes). Furthermore, the monthly distribution of widespread cases (table 1) shows that most of the “WS” cases occurred in June, and a few cases occurred in August.

In addition, the horizontal distribution of the TOMS AI (dust) for all selected summer episodes (figure 1-a) indicates that the dust covered northern Arabian Peninsula and continues to the Turkey border, but the highest dust values were concentrated over the eastern and southern Arabian Peninsula, which is considered a primary source of dust for the Arabian Peninsula and southern Red Sea (Mashat and Awad, 2010; Kalenderski et al., 2013). However,

the horizontal distribution of the widespread dust (figure 1-b) shows that the areas of highly concentrated summer dust extended from the main source areas to much of the Arabian Peninsula; the highest values occurred over the Red Sea. Additionally, high amounts of dust extended far north over most of Turkey.

MONTH	JUNE	JULY	AUGUST	TOTAL SUMMER EPISODES
NUMBER (RATIO)	**83 (45.6%)$_1$**	**68 (37.4%)$_1$**	**31 (17.0%)$_1$**	**182 (9.3%)$_2$**

Table 1. The number (percentage) of widespread episodes in summer (i.e., June, July and August) and the total number of episodes.
Subscript 1 indicates the ratio with respect to widespread episodes (182), while subscript 2 indicates the ratio with respect to the total selected dust episodes (1955 days).

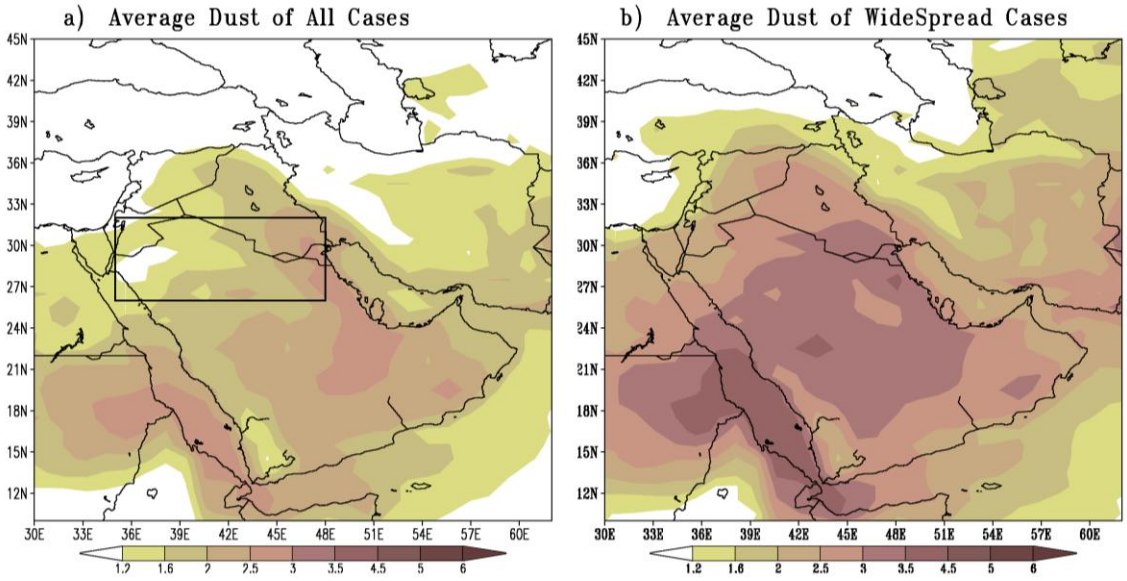

Figure 1. The maps represent (a) the horizontal distribution of the TOMS aerosol index (AI) for all selected dust episodes; the inner rectangle represents the location of the checking zone and its relative location with respect to the study area; and (b) the horizontal distribution of the TOMS AI values for the widespread episodes.

4.1. Statistical Analysis of Synoptic Features

The anomalies in the SLP field of widespread cases were statistically analyzed using an empirical orthogonal function (EOF), and the results show that the first ten EOF modes represented 77% of the widespread cases, while the first four EOF modes covered more than 52% of the cases. For simplicity and concentration, this study analyzed the synoptic features associated with the first four modes in detail.

The main distinguishing characteristics of these first four modes were the positive variations in the mean sea level pressure (SLP) for the first mode (figure 2-a), with a maximum variation in the SLP over the eastern Mediterranean, northern Arabian Peninsula and northern Europe. The positive SLP variations were replaced in the second mode by two regions of highly negative SLP variations in the western region and by relatively low positive SLP variations in the eastern region (figure 2-b). Furthermore, the maximum SLP variations in the second mode appeared in the north in both regions, which are far from the Arabian Peninsula.

In the third mode (figure 2-c), there are two main SLP variations regions, similar to the second mode; however, in this mode, the two regions were oriented north-south. Positive SLP variations occurred in the south, and a maximum variation occurred over the northeastern Mediterranean basin. Negative SLP variations occurred in the north, and a maximum variation occurred over Russia. In addition, in the third mode, there were two other regions with small positive and negative SLP variations that could be considered extensions of the main regions.

In the fourth mode (figure 2-d), there were four regions of SLP variations: two positive regions over the Arabian Peninsula and northwest and two negative regions over the west and northeast.

The description of the synoptic patterns that accompany these modes depends on choosing strong (weak) episodes that characterize these modes. These cases were represented by the extreme positive (negative) values in the PC modes (figure 3). These extreme positive (negative) values for the PC time series are the positive (negative) values that are greater (less) than the value that is equal to the absolute maximum (minimum) value plus half of the positive (negative) range, i.e., values above (below) the upper (lower) straight line in figure 3.

The composition of the chosen positive (negative) episodes of each mode represents the strong (weak) synoptic pattern activities that accompany this mode, similar to the relationship used by Trigo et al. (2000).

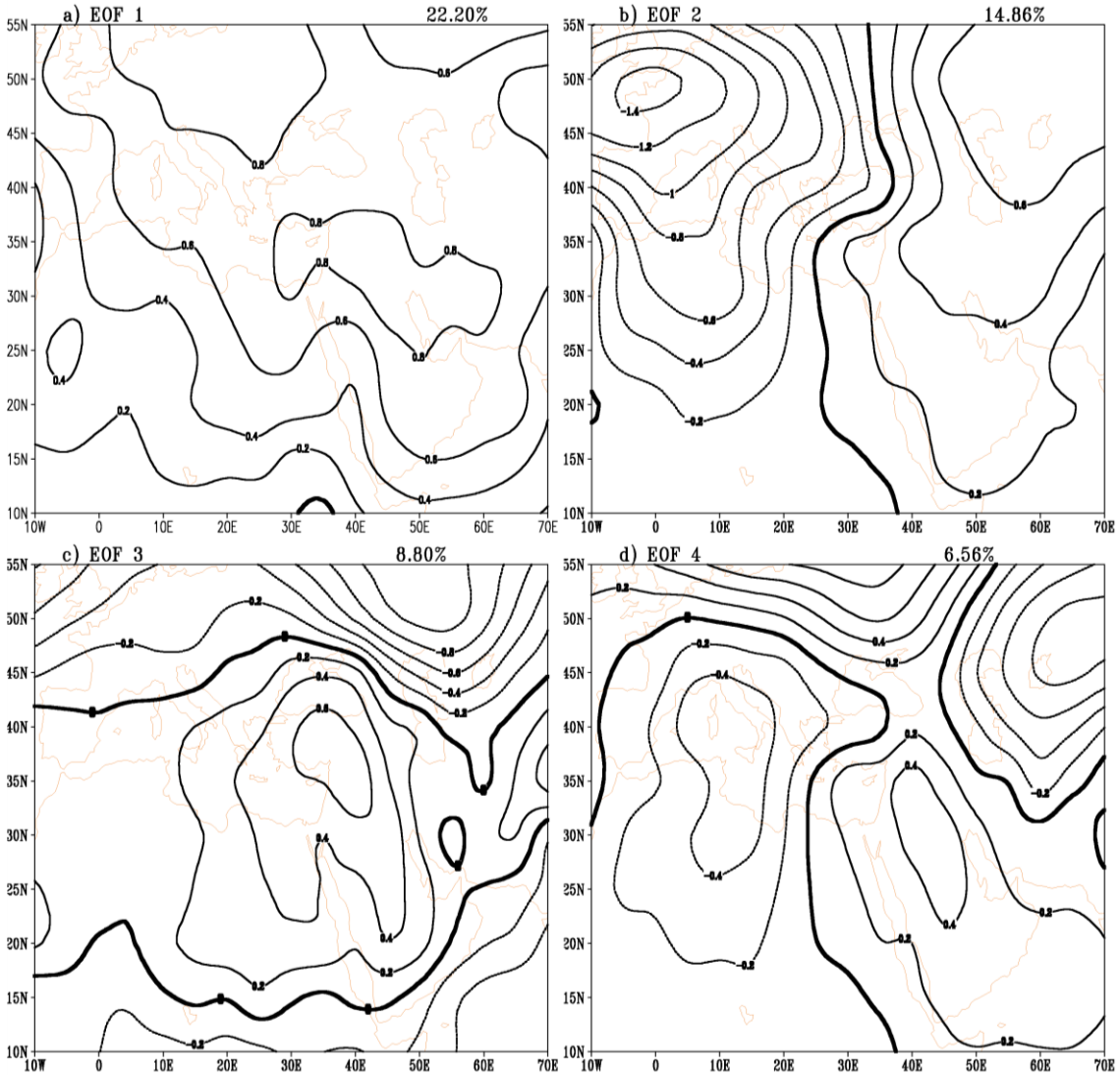

Figure 2. The distribution of SLP variations in the first four empirical orthogonal function analyses (EOF) modes for widespread summer dust episodes: (a) first, (b) second, c) third, and d) fourth EOF modes. The bold line represents a zero value.

4.2. Synoptic Compositions of the Patterns

4.2.1. First Pattern

As a strong (positive) pattern (figure 4-a), the strong Azores high, which had a core pressure of 1024 hPa, was located in the northwest. The Indian low, which had a core pressure of 1000 hPa, occurred over the Middle East. The Azores high influenced the Indian low through two ridges: a deep ridge that continued across the

Mediterranean and a short ridge that formed from a separate high-pressure cell over the Caspian Sea on the eastern side of the cyclonic system. Thus, a deep wave of ridges and troughs developed over the Arabian Peninsula.

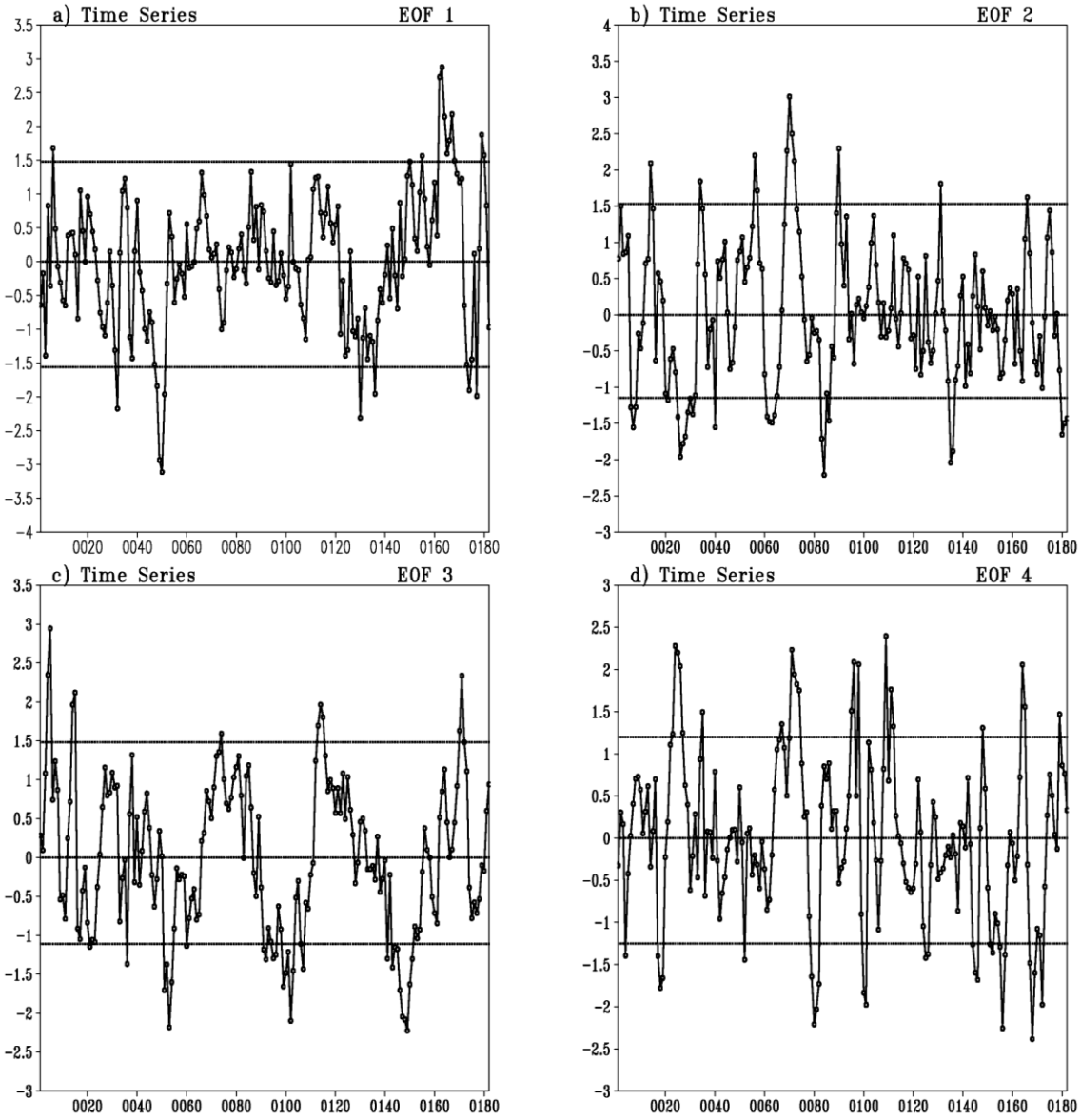

Figure 3. The time series of the four main principal components of the EOF analysis of the widespread summer dust episodes for the a) first, b) second, c) third, and d) fourth modes.

As a weak (negative) pattern (figure 4-b), there was a relatively weak Azores high in the west, with a maximum pressure of 1020 hPa. The Indian low over the Middle East had a minimum pressure of 994 hPa. The Azores high affected the Indian low through two ridges: a shallow ridge that directly extended over the Mediterranean Sea, and a deep ridge that formed from a separate high-pressure cell over the Black and Caspian Seas on the eastern side of the Indian low. As a result, a strong and deep trough developed over the Arabian Peninsula.

In addition, the maximum wind at 250 hPa shows the wind increase for the strong pattern (figure 4-a) than the weak pattern (figure 4-b). Additionally, the distribution of the AI shows that for the strong pattern, the AI was distributed over small areas (figure 4-c), while for the weak pattern, the AI (figure 4-d) was distributed over large areas.

At the 850 hPa pressure level, the synoptic features distinguished the strong pattern (figure 5-a), with an anticyclonic system in the west (1580 gpm) and a cyclonic system in the southeast (1430 gpm). In addition, there were two weak systems: an anticyclonic cell over the Caspian Sea (1530 gpm) and a cyclonic system in the northeast (1480gpm).

The interaction of the strong and weak anticyclones and the northeastern cyclone with the main cyclone produced a distinct wave over the Arabian Peninsula and a deep cyclonic trough east of the Arabian Gulf.

For the weak pattern (figure 5-b), the atmospheric systems were similar to those of the strong pattern. The deepening of the main cyclone, weakening of the main anticyclone, and the change in the location of the weak cyclone reoriented the cyclonic trough west, relocated the trough over the eastern Arabian Peninsula, and smoothed the wave over the Arabian Peninsula.

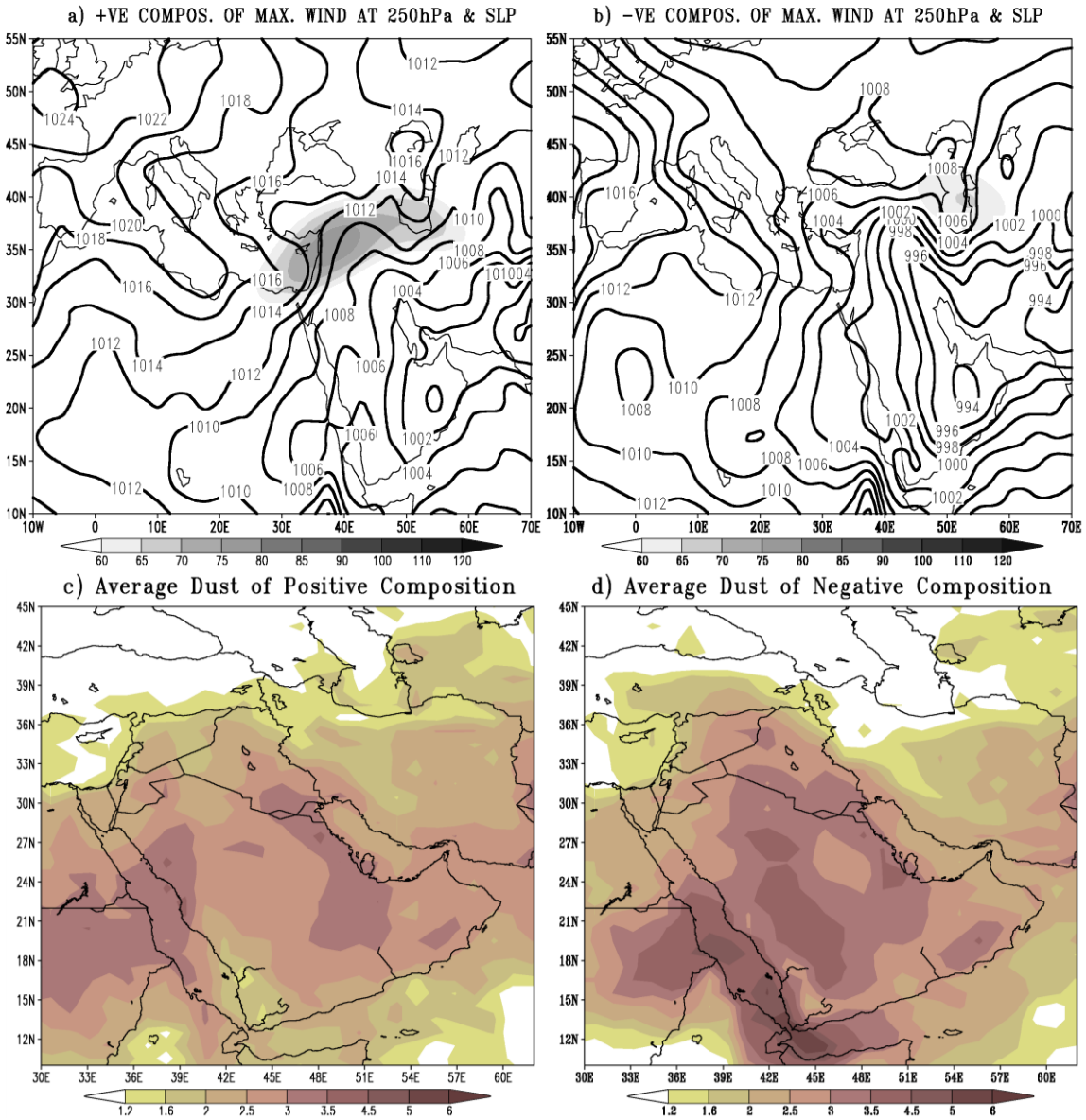

Figure 4. The distribution of the mean sea level pressure (SLP) (contours) and maximum wind speed at 250 hPa (shaded) for the composition of the first synoptic pattern for (a) strongly active cases and (b) weakly active cases; the horizontal distribution of the TOMS AI values for the composition of (c) strongly active cases and (d) weakly active cases.

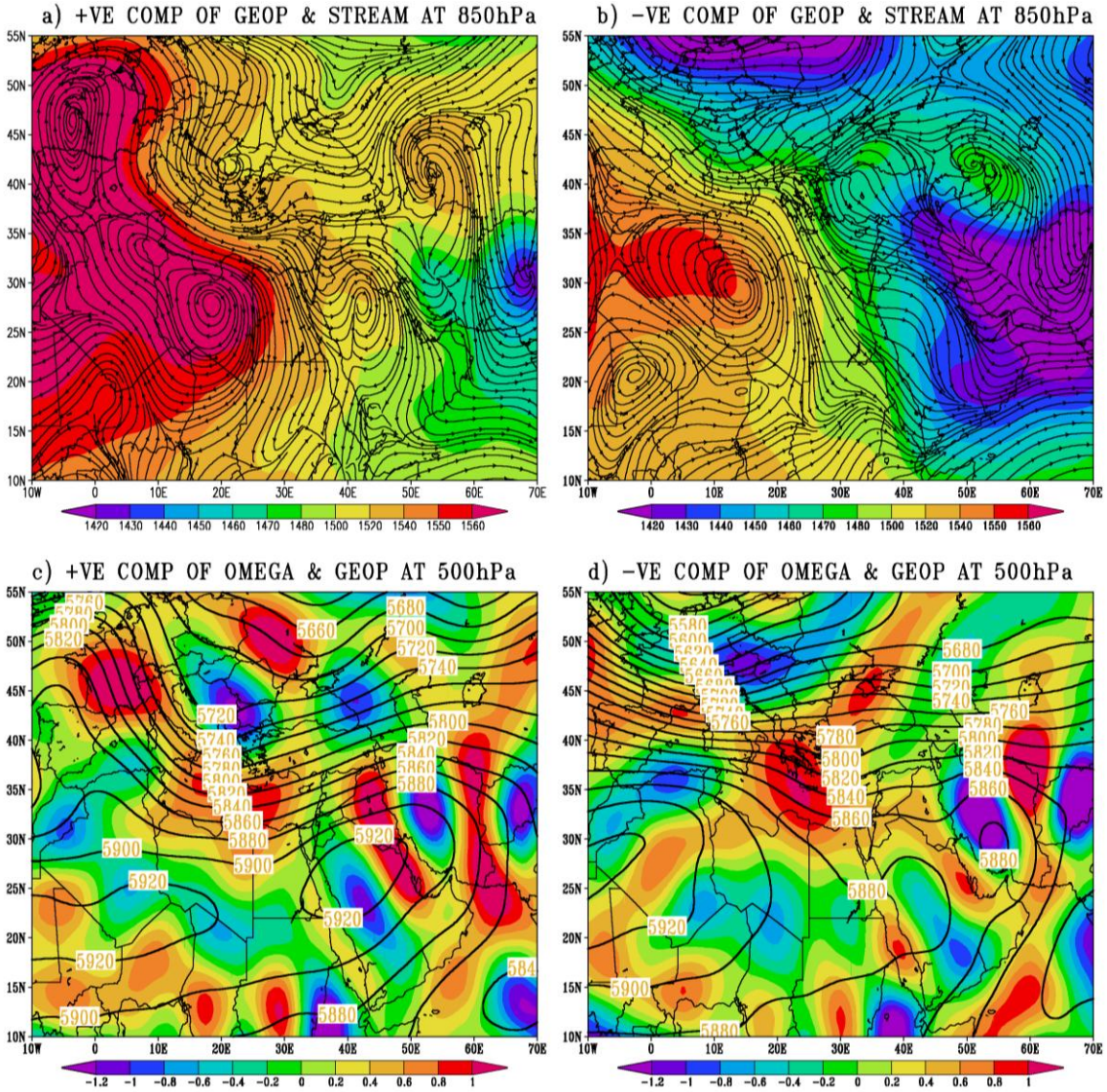

Figure 5. For the first synoptic pattern, the distribution of the geopotential heights (shading) and streamlines at 850 hPa (contours) for (a) strongly active cases and (b) weakly active cases; the geopotential heights (contours) and the vertical motion at 500 hPa (shading) for (c) strongly active cases and (d) weakly active cases.

For the wind at the 850 hPa pressure level, which distinguished the strong pattern (figure 5-a) and the weak pattern (figure 5-b), there were many anticyclonic and cyclonic wind patterns for the strong pattern that formed a shortwave wind distribution. Additionally, there was only an anticyclonic wind pattern over the Arabian Peninsula for the strong pattern, which produced northwesterly and southwesterly wind over the northwestern Arabian Peninsula and northerly wind over the northeastern Arabian Peninsula, respectively.

The atmospheric systems at the 500 hPa pressure level were the cyclonic system over the north and the anticyclonic system over south. A strong gradient and wave shape were apparent in the strong pattern, which transitioned to a flat, weak gradient in the weak pattern.

In the strong pattern (figure 5-c), the main cyclonic center was located over North Europe, with a minimum height of 5640 gpm; a trough was oriented northwest to southeast, influencing the eastern Mediterranean. The anticyclonic system had a high-pressure cell over the Arabian Peninsula, with a maximum height of 5920 gpm; a ridge was oriented southwest to northeast. In the weak pattern (figure 5-d), the cyclonic center was located over

Northwest Europe, with a minimum height of 5540 gpm; a trough was oriented north to south over the eastern Mediterranean and Red Sea. The anticyclonic system was associated with a ridge over the Arabian Peninsula, with a maximum height of 5880 gpm, and a high-pressure cell over Iran, with a maximum height of 5880 gpm.

In addition, the vertical motion at this level for a strong pattern (figure 5-c) shows a sequence of rising motion and subsidence over the Arabian Peninsula, starting with rising motion in the west and large-scale subsidence over the Mediterranean and North Africa. For the weak pattern, the subsidence over the Arabian Peninsula weakened (figure 5-d), while the subsidence over the Mediterranean and North Africa strengthened and flattened. In general, the vertical motion on the small scale was associated with a strong pattern rather than a weak synoptic pattern.

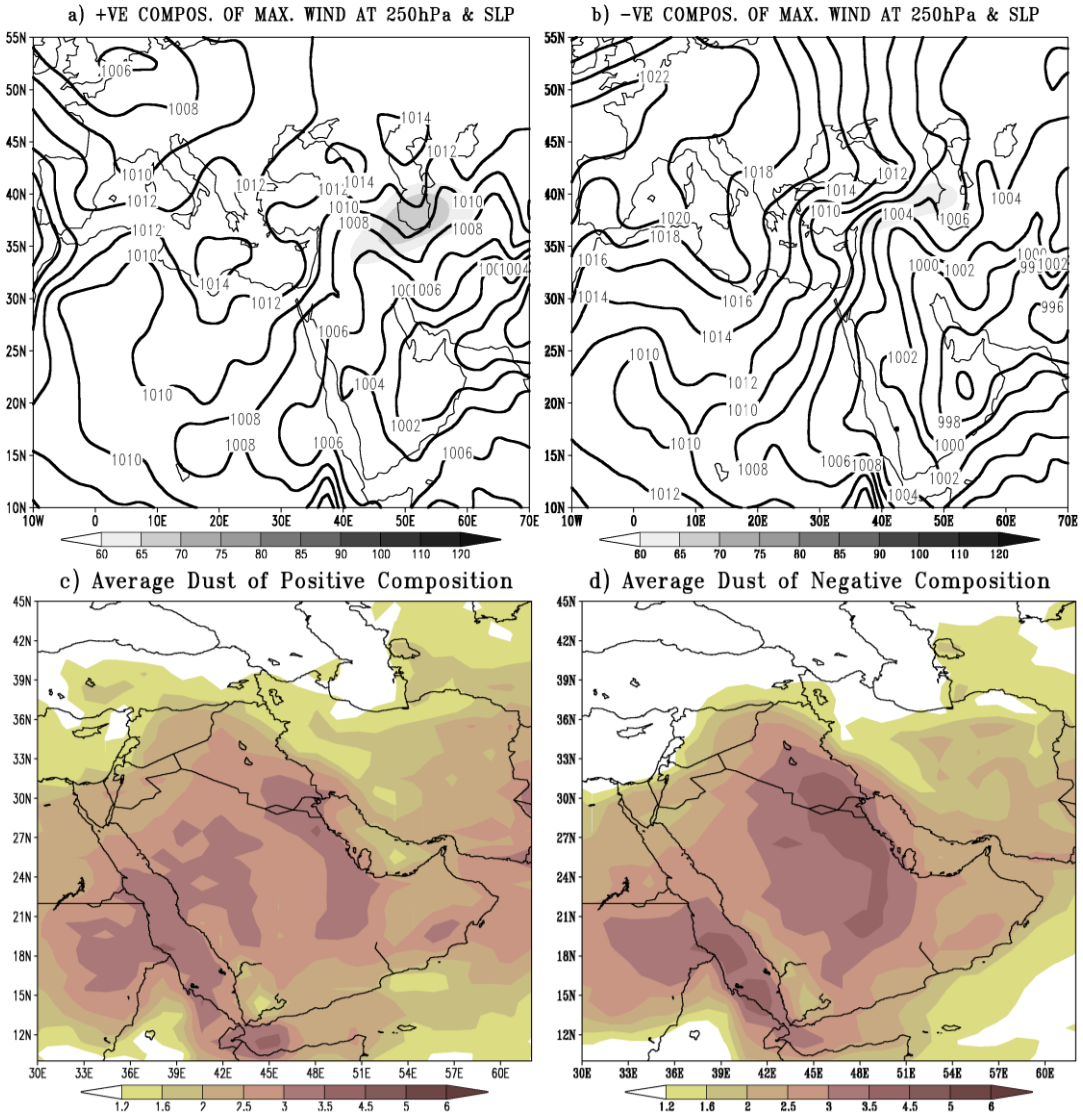

Figure 6. As in Figure 4 but for the second synoptic pattern.

4.2.2. Second Pattern

For the strong pattern (figure 6-a), the main synoptic features were two low-pressure systems: the Indian low pressure in the east (998 hPa) and a low pressure system over northwestern Europe (1006 hPa). In addition, there were two high-pressure cells: one over the Mediterranean and the other over the Caspian Sea, both of which had a pressure of 1014 hPa.

Both of the high-pressure cells influenced the Indian low pressure and produced wavy ridges and troughs over the greater Arabian Peninsula; additionally, the spatial distribution extended the Indian low pressure northward.

In the weak representative (figure 6-b), the main synoptic features were two large-scale systems: the Azores high in the west (1022 hPa) and the Indian low pressure in the southeast (996 hPa). The Azores high had two ridges that both affected the Indian low pressure over the Arabian Peninsula; one ridge impacted the Mediterranean and the other ridge impacted the eastern side of the Indian low pressure. The distribution of high-pressure systems prevented the Indian low pressure from extending northward and from producing a low-pressure southeast-northwest trough.

In addition, the maximum wind at 250 hPa decreased more in the weak representative (figure 6-b) than in the strong representative (figure 6-a). Additionally, similar to the first representative , the AI had small areas of high values for the strong representative (figure 6-c) but large areas for the weak representative (figure 6-d).

The synoptic structures of the strong representative at the 850 hPa pressure level (figure 7-a) were cyclones over the southeastern and northwestern regions, with minimum heights of 1430 and 1410 gpm, respectively. Additionally, two anticyclonic cells developed over Libya and the eastern Caspian Sea, with maximum heights of 1540 and 1530 gpm, respectively. A very small anticyclonic cell of 1510 gpm was found over the northern Arabian Peninsula. This structure formed a large trough-ridge pattern over the peninsula and northward.

In the weak representative (figure 7-b), the anticyclonic system (1580 gpm) was pronounced over the western region, while the cyclonic system (1400 gpm) was pronounced over the eastern region. In addition, a ridge from the western anticyclone affected the eastern Caspian Sea and formed a deep trough over the eastern Arabian Gulf by interacting with the cyclonic system. Additionally, in this case, the strength of the western anticyclone and the strong eastern cyclone smoothed the deep wave in the positive scenario.

The wind distribution at this level shows that over the northwestern region, the cyclonic wind pattern was pronounced in the strong representative,(figure 7-a), and the anticyclonic wind pattern was pronounced in the weak representative,(figure 7-b). Moreover, in the strong case, many of the streamline centers produced a short streamline wave and northwesterly, southwesterly and northerly winds from the west to east over the Arabian Peninsula.

As seen in the first synoptic pattern, two atmospheric systems influenced the 500 hPa pressure level; however, in the strong representative (figure 7-c), the cyclonic system was centered over northeastern Europe, with a minimum height of 5640gpm; a trough was oriented north to south. The southern anticyclone had a high-pressure cell, with a maximum height of 5900 gpm, over the Arabian Peninsula.

In the weak representative, (figure 7-d), the northern cyclone shifted eastward toward Russia and formed a trough from northeast to southwest over the eastern Mediterranean. The anticyclonic system had a high-pressure cell (5920 gpm) over the Arabian Peninsula.

The subsidence over the Mediterranean and North Africa in the strong representative, (figure 7-c), extended southward and formed a subsidence cell over eastern Africa. Additionally, a sequence of subsidence and rising motion formed over the Arabian Peninsula and adjacent areas. In the weak representative, (figure 7-d), the southern extent of the subsidence over the Mediterranean and North Africa weakened, and the vertical motion weakened, except for the rising motion over Iran, which intensified and extended northward.

4.2.3. Third Pattern

In the strong representative, (figure 8-a), there were two main pressure systems controlling the surface systems: the Azores high in the northwest (1020 hPa) and the Indian low pressure in the southeast (996 hPa). In addition, there were weak low-pressure systems over the Sahara (1010 hPa) and the northeast (1006 hPa). The Azores high affected the Indian low through the ridge over the Mediterranean and the ridge over the Caspian Sea, but the northeastern low-pressure cell reduced the effect of the Caspian ridge by strengthening the connection with the Indian low. The final result was an elongated trough in the northern Arabian Peninsula and Levant regions.

In the weak representative, (figure 8-b), the Indian low pressure in the southeast (998 hPa) was connected to the Saharan low, producing a low-pressure belt over the south. The Azores high in the northwest (1020 hPa) extended eastward and connected with high pressure over the northeast (1018 hPa), producing a high-pressure belt in the north.

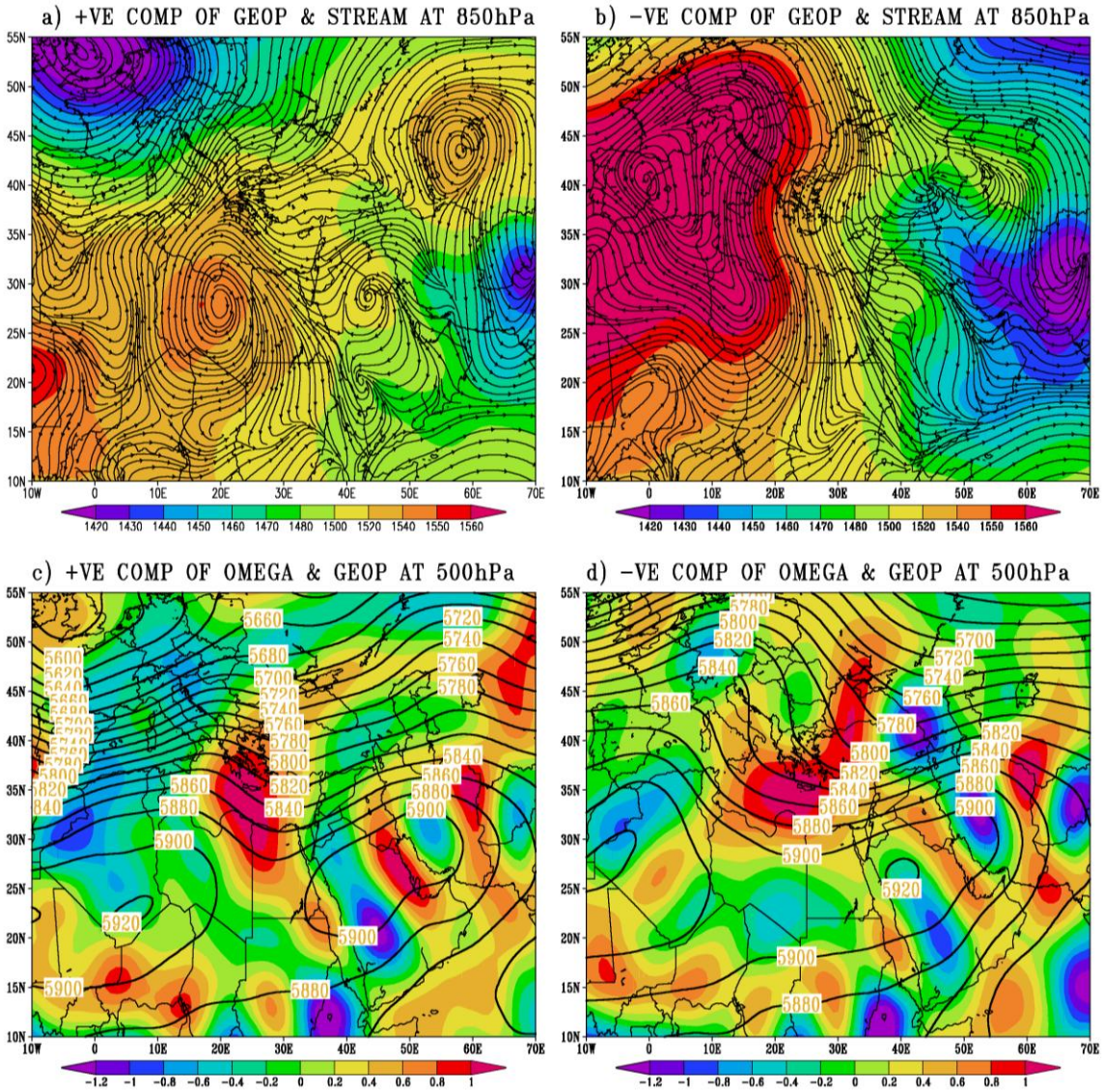

Figure 7.As in Figure 5 but for the second synoptic pattern.

In this representative, the Indian low pressure extended between the two high-pressure systems to produce a deep and sharp trough over the northern Arabian Peninsula.

However, the maximum wind at 250 hPa shows that the wind was stronger in the strong representative, (figure 8-a), than in the weak representative,(figure 8-b).

Additionally, the aerosol index was distributed over small areas in the strong representative, (figure 8-c), and large areas in the weak representative, (figure 8-d).

In the strong representative at the 850 hPa level (figure 9-a), a pronounced deep cyclone influenced the entire northern region, and a cyclonic system (1420 gpm) affected the eastern region, and an anticyclonic system (1560 gpm) impacted Libya. Additionally, an anticyclonic cell, with a maximum closed contour of 1510 gpm, was found over the eastern Caspian Sea. This atmospheric pattern formed a deep wave over the Arabian Peninsula and Levant.

In the weak representative at the 850 hPa pressure level (figure 9-b), a pronounced anticyclonic system (1560 gpm) was found over the northeastern region. Furthermore, an anticyclonic system (1570 gpm) affected the western region, and a cyclonic system (1410 gpm) developed over the southeast. This synoptic structure formed a deep cyclonic trough over the Arabian Peninsula that extended northward over the northern Black Sea and smoothed the deep wave in the strong representative.

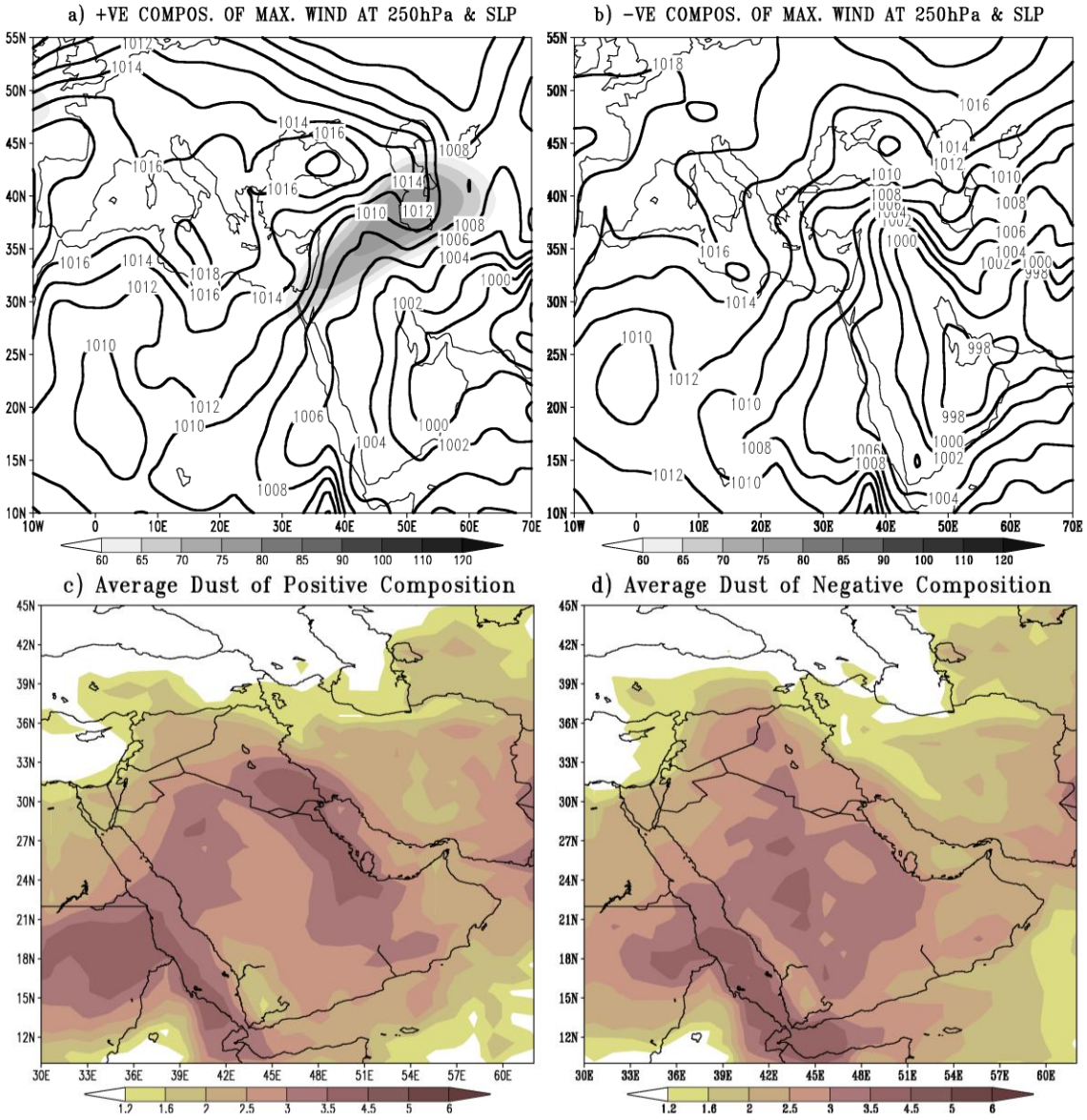

Figure 8. As in Figure 4 but for the third synoptic pattern.

The main difference in the wind streamlines at 850 hPa between the representatives (figure 9) is that in the weak representative, (figure 9-b), the structure was larger scale than that in the strong representative (figure 9-a). Additionally, the anticyclonic pattern over Africa was small scale and eastward in the strong representative (figure 9-a), and the cyclonic pattern in the northeast was southward in the weak representative, (figure 9-b). Furthermore, a small-scale anticyclonic wind pattern occurred over the middle Arabian Peninsula in the strong representative, (figure 9-a), in which small-scale wind features formed over the northern Arabian Peninsula.

At the 500 hPa pressure level, for the strong representative, (figure 9-c), the north cyclone was centered over Russia, with a minimum height of 5540 gpm, and the trough was oriented northeast to southwest. The anticyclone, which had a maximum height of 5900 gpm, influenced the Arabian Peninsula and formed a ridge oriented southwest to northeast. In the weak representative, (figure 9-d), the center of the northern cyclone was located over the northwest, with a minimum height of 5600 gpm. A trough was oriented north to south across the eastern Mediterranean, while the southern anticyclone (5900 gpm) formed a ridge oriented southwest to northeast.

In the strong representative, (figure 9-c), vertical motion appeared over the Arabian Peninsula, where subsidence cells extended from the subsidence region over the Mediterranean and Russia. In the weak representative, (figure 9-d), the subsidence over Russia was converted to rising motion, which weakened the subsidence cell over the eastern Arabian Peninsula. In addition, the subsidence over the Mediterranean and North Africa was dampened and not strongly connected with the subsidence over the Red Sea.

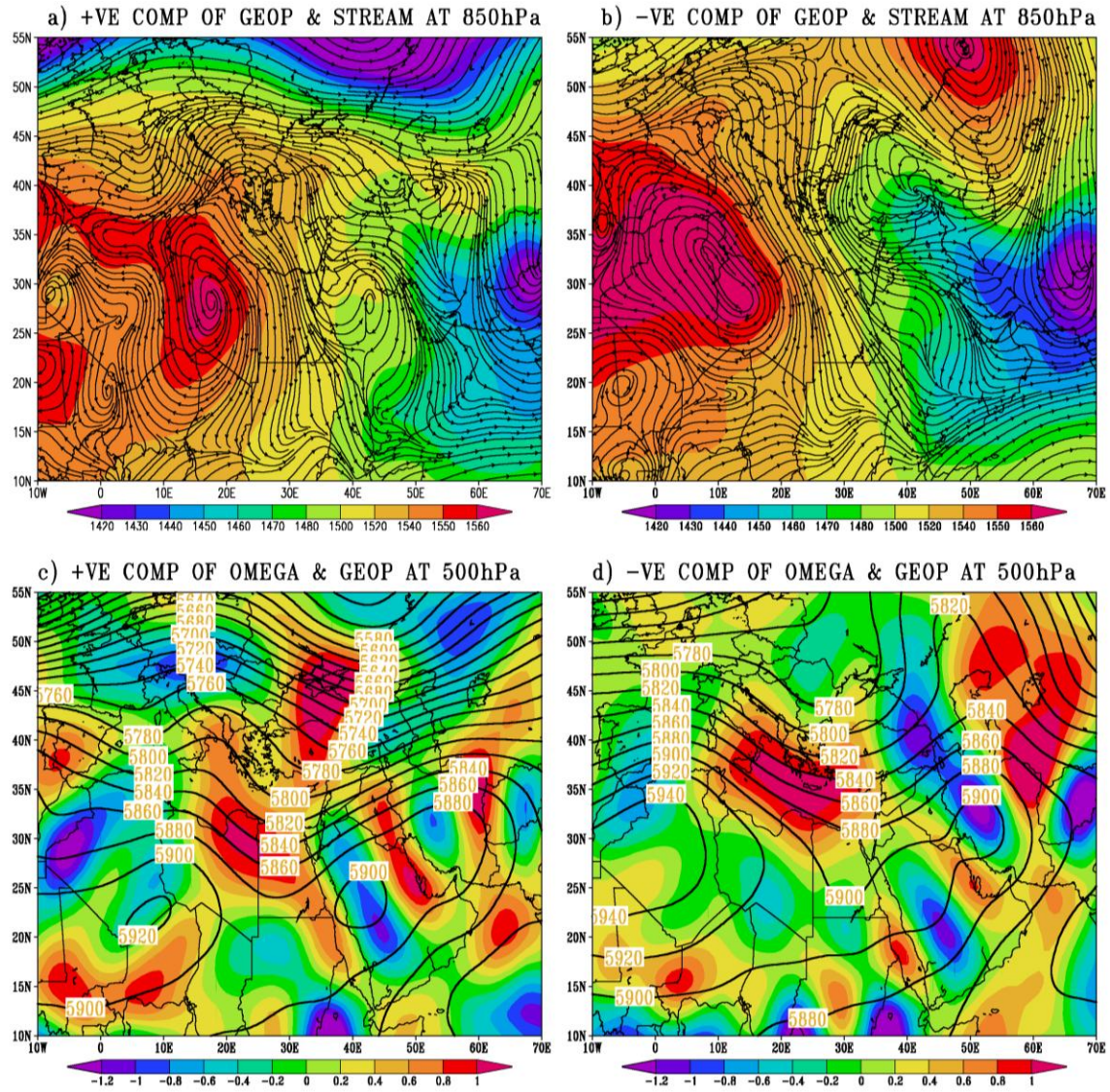

Figure 9.As in Figure 5 but for the third synoptic pattern.

4.2.4. Fourth Pattern

In the strong representative (figure 10-a), the Indian low (998 hPa) merged with the Azores high (1018 hPa), forming a wave pattern over the Arabian Peninsula. In this, representative another core of high pressure appeared over northern Europe. Additionally, the Indian low connected with the low-pressure system over the Sahara.

In the weak representative, (figure 10-b), the Indian low deepened to 996 hPa, and the Azores high intensified to 1020 hPa. Coupled with the previous systems, relatively weak low pressure (1008 hPa) appeared over northeastern Europe, and weak high pressure (1016 hPa) occurred in the northeast extremity. Furthermore, the Indian low formed a deep and sharp trough over the Arabian Gulf and Peninsula, while a weak wave connected with the Azores high.

Additionally, the maximum wind at 250 hPa shows that the wind was stronger in the weak representative, (figure 10-b), than in the strong representative,(figure 10-a). Whiles, the aerosol index was distributed over small areas in the strong representative, (figure 10-c), and large areas in the weak representative, (figure 10-d).

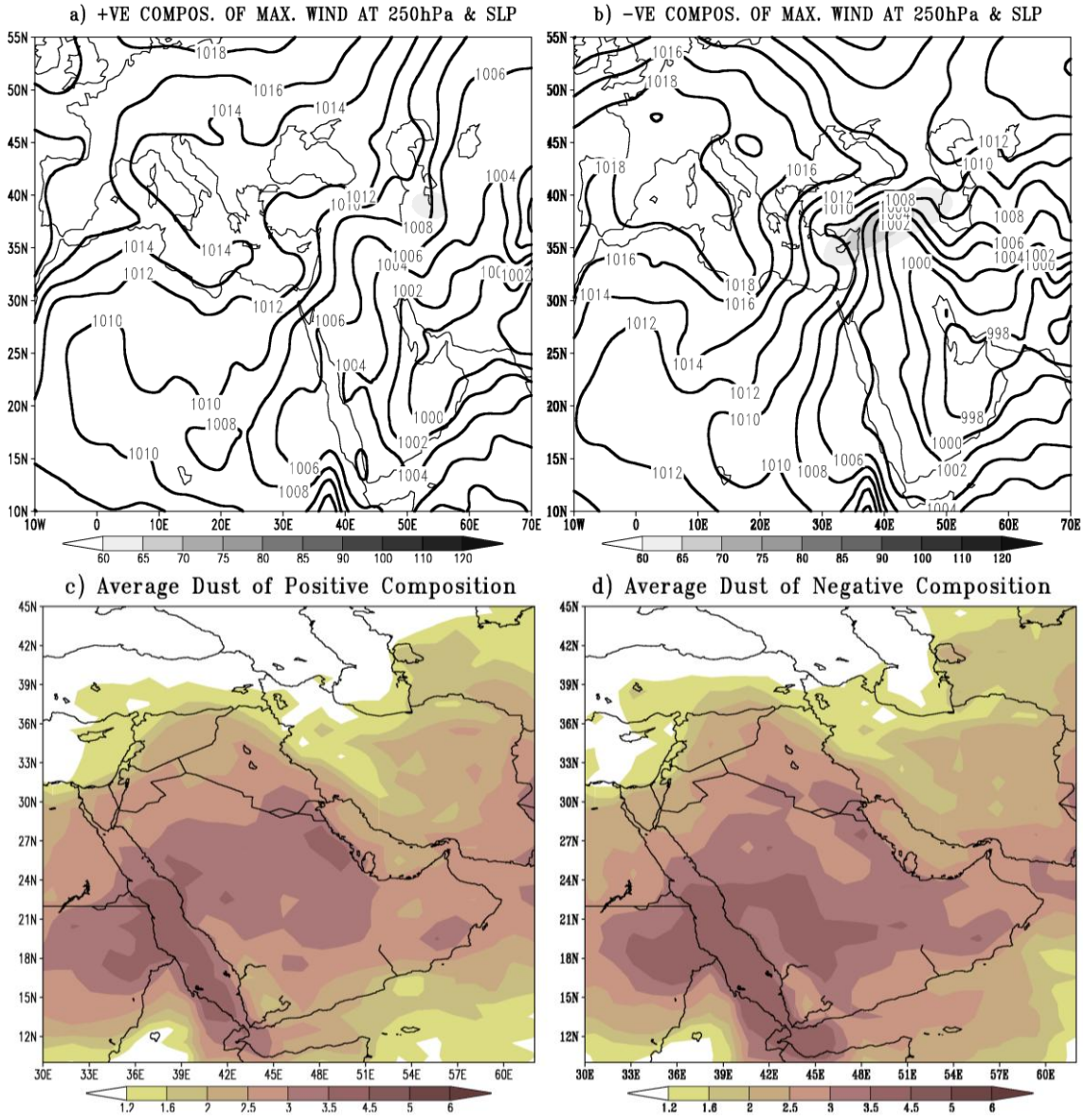

Figure 10. As in Figure 4 but for the fourth synoptic pattern.

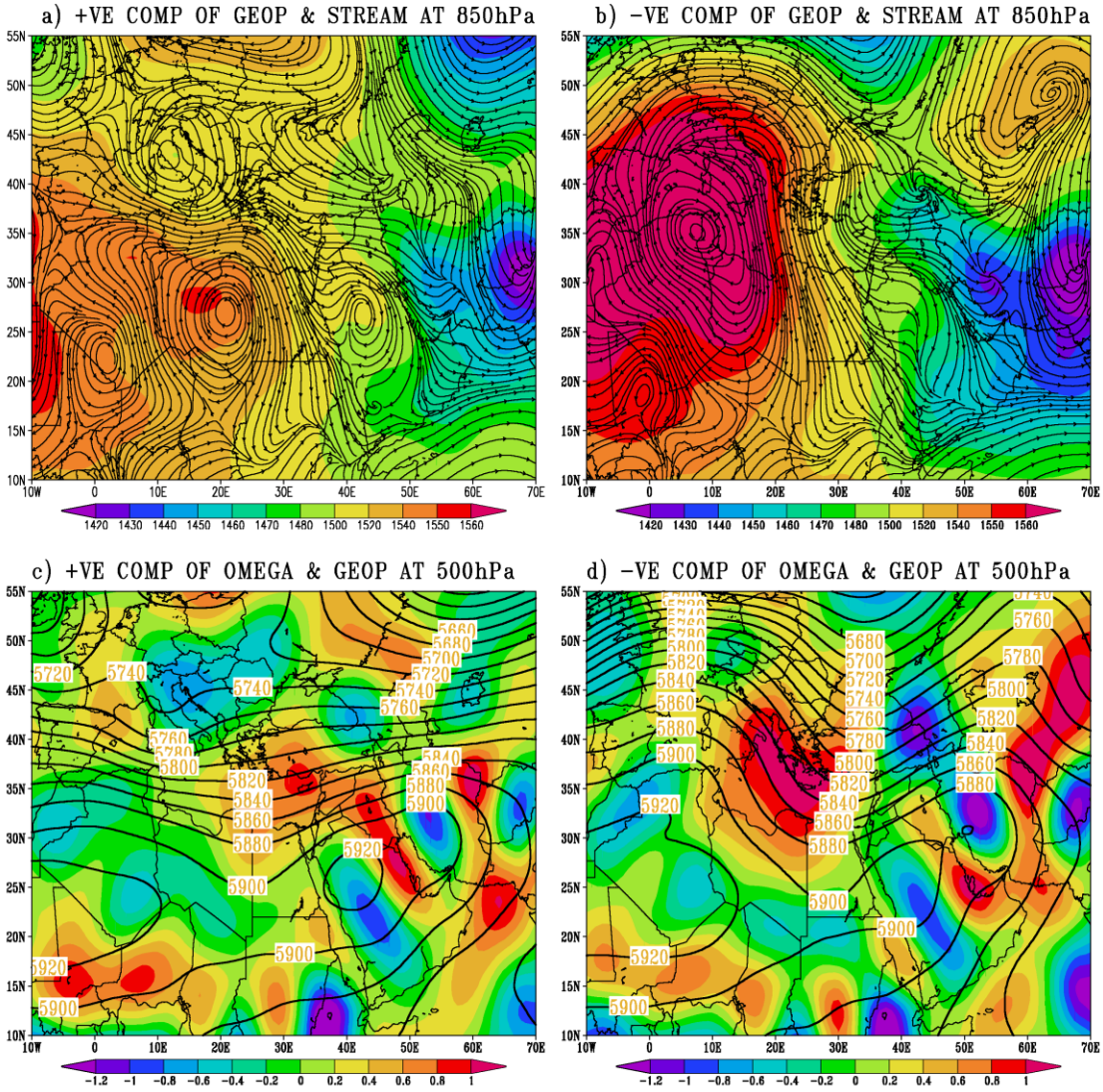

Figure 11.As in Figure 5 but for the fourth synoptic pattern.

In the strong representative at the 850 hPa pressure level (figure 11-a), a sequence of small cyclones and anticyclones affected the northern region. An anticyclone formed over Libya (1550 gpm), and a cyclone formed over the east (1420 gpm). A weak ridge affected the eastern Arabian Gulf. The interaction between the cyclonic and anticyclonic systems formed a deep wave over the Arabian Peninsula and the region to the north.

The atmospheric structures in the strong representative were repetitive in the weak representative, (figure 11-b), and a deep trough developed between the systems over Iran, the Arabian Peninsula and Levant. Additionally, this structure smoothed the deep wave in the strong representative.

The main features distinguishing the representatives were the wind patterns found at small scales and the anticyclonic pattern over the Sahara in the strong representative, (figure 11-a), which was southeast of that in the weak representative,(figure 11-b). In addition, an anticyclonic wind pattern found in the strong representative over the Arabian Peninsula (figure 11-a) did not exist in the weak representative, (figure 11-b), which formed small-scale features in the streamlines over the northern Arabian Peninsula.

Although the atmospheric systems at the 500 hPa pressure level were similar to those in the previous pattern, in the strong representative, (figure 11-c), there were two cyclonic systems. The first system was over the northeast region (5600 gpm), and the second system was over the northwest region (5660 gpm); these systems formed a north-south trough that influenced the Mediterranean. In addition, the southern anticyclone (5920 gpm) influenced the Arabian Peninsula and formed a west-east ridge. In the weak representative, (figure 11-d), the

northern cyclone (5620 gpm) was located over northeastern Europe; it formed a north-south trough. The southern anticyclone(5900 gpm) influenced the Arabian Peninsula and formed a southwest-northeast ridge.

In addition to the vertical motion in the strong representative, (figure 11-c), a subsidence area occurred over the northeast corner of the Mediterranean, which was connected with the subsidence over the eastern Arabian Peninsula but was weakly connected with the subsidence over the Red Sea. However, in the weak representative, (figure 11-d), the rising motion over Russia shifted the subsidence over the Mediterranean westward and weakened its connection with the subsidence over the eastern Arabian Peninsula.

5. Discussion and Conclusions

This study examined the synoptic features of widespread dust episodes over the northern Arabian Peninsula in summer. All of the summer dust cases were first selected using an AI threshold of 2.0; then, the widespread cases were chosen under the condition that 70% of the grid points within the checking zone achieved this threshold value. The results show that much of the summer (82%) was dusty, but a few of the cases were widespread (9.3%). Most of these widespread cases occurred in June and gradually decreased toward the end of the summer.

A statistical EOF analysis of the SLP associated with the widespread cases demonstrated that the first four modes cover more than 52% of the cases, which represented the most pronounced synoptic patterns. The pressure systems associated with these patterns indicated a high ratio of dust cases when a strong and large-scale system influenced the region, while the ratio decreased when two large systems were in the vicinity and were distributed east-west. Moreover, the ratio continued to decrease when the two systems were distributed north-south. The minimum ratio occurred when four systems influenced the region and formed a crosswise pattern.

In the strong representative of the first pattern, the Azores high merged with a relatively weak Indian low, forming a deep wave over the Arabian Peninsula. In the weak representative the deep Indian low was less affected by the Azores high, which smoothed the wave over the Arabian Peninsula; however, it was highly influenced by the ridge of the high-pressure cell in the east.

For the second pattern, the pressure systems in the strong representative produced a large wave over the Arabian Peninsula and extended the Indian low pressure northward. In the weak representative, the Azores high did not produce a pronounced wave over the Arabian Peninsula but did promote a southeast-northwest Indian low trough.

In the strong representative of the third pattern, the existence of low pressure over the northeast reduced the effect of the Azores high on the Indian low pressure and flattened the trough over the Arabian Peninsula. In the weak representative, the northeastern high pressure combined with the Azores high to produce a deep and sharp trough over the Arabian Peninsula.

In the strong representative of the fourth pattern, two neighboring high-pressure cores allowed the Indian low pressure to form a deep wave over the Arabian Peninsula and adjacent region. In the weak representative, the separation between the high-pressure cores and the strength of the Azores high allowed the Indian low to form a sharp and deep trough over the Arabian Peninsula, which extended northward into Turkey.

Although the synoptic structures at the 850 hPa pressure level conformed to the characteristics of the surface patterns, the streamlines showed that the wind patterns in the strong representative were smaller scale than those in the weak representative. Additionally, the scale of the wind patterns was inverse proportional to the frequency of the synoptic pattern, for which the scale was the smallest for the first synoptic pattern. In the strong representative, there was an anticyclonic wind pattern over the northern Arabian Peninsula that produced a shortwave and northwesterly, southwesterly and northerly winds over the northern Arabian Peninsula from west to east.

Furthermore, the atmospheric systems at the 500 hPa pressure level demonstrated that the trough of the northern cyclone was oriented clockwise from a high-frequency pattern to a low-frequency pattern. The geopotential field formed a wave that had a strong gradient in the strong representative and a weak gradient in the weak representative. Additionally, the vertical motion was distributed over a smaller scale in the strong representative compared with the weak representative. A sequence of rising motion and subsidence formed over the Arabian Peninsula. In addition, the subsidence cell over the central Arabian Peninsula intensified as the frequency of the atmospheric patterns increased, while the subsidence over the Mediterranean and North Africa decreased more in the strong representative than in the weak representative.

Therefore, the system that is most strongly related to dust over the northern Arabian Peninsula is the pronounced Indian low pressure in summer. Along with this system is the western Azores high pressure, which

merges with the Indian low in many ways; the unique pressure patterns are associated with dust over the region. The four most pronounced patterns are as follows: the frequent one appeared when high pressure system is strong and dominated, while the less frequent one appeared when Indian low pressure is strong and dominated; and two moderate patterns whose strength depends on the proximity to an extreme pattern.

Generally, from the synoptic analysis of the main patterns, two factors control the widespread cases over the region. The first factor is related to the scale of the pressure systems over the region, where the frequency of cases is proportional to the system scale. The second factor is related to the interaction between the Azores high pressure and the Indian low pressure, where a strong representative appeared when the two systems formed a deep wave over the Arabian Peninsula and a weak representative appeared when the Indian low pressure formed a deep and sharp trough rather than a pronounced wave with the Azores high pressure.

References

Adel M. Awad 2014: Characteristics of Atmospheric Systems Accompany with Summer Dust over Northern Arabian Peninsula. Int. J. of Adv. Res. 2 (12), 821-833. (ISSN 2320-5407) www.journalijar.com.

Awad AM and Abdul-Wahab S. Mashat 2014-a: Synoptic Features Associated with Dust Transition Processes from North Africa to Asia, Arabian Journal of Geosciences, 7(6): 2451-2467; doi:10.1007/s12517-013-0923-4

Awad AM, Mashat AS, Abo Salem FF 2014: Diagnostic study of spring dusty days over the southwest region of the Kingdom of Saudi Arabia. Arab J Geosci. doi:10.1007/s12517-014-1318-x.

AwadA; Mashat, Abdul-Wahab. 2014-b: The Synoptic Patterns Associated with Spring Widespread Dusty Days in Central and Eastern Saudi Arabia. Atmosphere 5, no. 4: 889-913.

Barkan J.; Alpert, P. 2008: Synoptic patterns associated with dusty and non-dusty seasons in the Sahara. Theor. Appl. Climatol., 94, 153–162.

Crosbie, E., Sorooshian, A., Monfared, N.A., Shingler, T., Esmaili, O., 2014: A multi-year aerosol characterization for the greater Tehran Area using satellite, surface, and modeling data, Atmosphere, 5, 178-197

Gkikas, A.; Houssos, E.E.; Hatzianastassiou, N.; Papadimas, C.D.; Bartzokas, A. Synoptic conditions favouring the occurrenceof aerosol episodes over the broader Mediterranean basin. Q.J.Roy. Meteorol. Soc.2012, 138, 932–949.

Hamidi, M.; Mohammad, R.K.; Yaping, S. Synoptic analysis of dust storms in the Middle East.Asia-Pacific J. Atmos. Sci.2013, 49, 279–286.

Herman JR, Bhartia PK, Torres O, Hsu C, Seftor C, Celarier E, 1997: Global distribution of UV-absorbing aerosols from Nimbus-7/TOMS data. *J Geophys Res 102:16,911–16,922.*

Hsu NC, Herman JR, Torres O, Holben BN, Tanre D, Eck TF, Smirnov A, Chatenet B, Lavenu F. , 1999: Comparisons of the TOMS aerosol index with sun-photometer aerosol optical thickness: results and applications. J. Geophys. Res. 104:6269–6279.

Jolliffe, I.T. Principal Component Analysis; Springer: New York, NY, USA, 1986.

Kalendarski, S.; Stenchikov, G.; Zhao, C. Modeling a typical winter-time dust event over the Arabian Peninsula and the Red Sea. Atmos. Chem. Phys. 2013, 13, 1999–2014.

Kalnay E, Kanamitsu M, Kistler R, Collins W, Deaven D, Gandin L ,IridellM, Saha S, White G, WoollenJ,Zhu Y ,Chelliah M, Ebisuzaki W, Higgins W ,JanowiakJ,Mo KC, Ropolewski C, Wang J, Leetma A, Reynolds R, Jenne R, Joseph D., 1996: The NCEP/NCAR 40-year Reanalysis project. Bull Am MeteorolSoc 77: 437–471

Kim, D., Chin, M., Yu, H., Eck, T.F., Sinyuk, A., Smirnov, A., Holben, B.N., 2011: Dust optical properties over North Africa and Arabian Peninsula derived from the AERONET dataset.Atmos. Chem. Phys. Discuss. 11, 20181–20201.

Kistler R, Collins W, Saha S, White G, Woollen J, Kalnay E, Chelliah M, Ebisuzaki W, Kanamitsu M, Kousky V, vandenDool H, Jenne R, Fiorino M., 2001: The NCEP/NCAR 50-year Reanalyses: Monthly CD-ROM and documentation. Bull Am MeteorolSoc 82: 247–267.

Maghrabi, A., Alharbi, B., Tapper, N., 2011. Impact of the March 2009: dust event in Saudi Arabia on aerosol optical properties, meteorological parameters, sky temperature and emissivity. Atmos. Environ. 45, 2164-2173.

Mahowald NM, Luo C, delCorralJ and Zender C., 2003: Interannual variability in atmospheric mineral aerosols from a 22-year model simulation and observation data. J Geophys Res 108 (D12).doi: 10.1029/2002 JD002821.

Manly, B.F.J. Multivariate Statistical Methods: A Primer; Chapman & Hall: London, UK, 1986.

Mashat Abdul Wahab, Awad A. M.2010: The Classification of the Dusty areas over the Middle-East. Bull. Fac. Sci., Cairo Univ. 78(A): 1-19.

Smirnov, A., Holben, B.N., Dubovic, O., O'Neill, N.T., Eck, T.F., Westphal, D.L., Goroth, A.K., Pietras, C., Slutsker, I., 2002: Atmospheric aerosol optical properties in the Persian Gulf. J. Atmos. Sci. 59, 620-634.
Torres O, Bhartia PK, Herman JR, Ahmad Z, Gleason K., 1998: Derivation of aerosol properties from satellite measurements of backscattered ultraviolet radiation: theoretical basis. J Geophys Res 103: 17099–17110.
Trigo, I. F., T. D. Davies, and G. R. Bigg, 2000: Decline in Mediterranean rainfall caused by weakening of Mediterranean cyclones. Geophys. Res. Lett., 27, 2913–2916.